Role of disorder in incorporation energies of oxygen atoms in amorphous silica

Marek A. Szymanski,[1,2] Alexander L. Shluger,[1] and A. Marshall Stoneham[1]
[1]*Department of Physics and Astronomy, University College London, Gower Street, London WC1E 6BT, United Kingdom*
[2]*Faculty of Physics, Warsaw University of Technology, ul. Koszykowa 75, 00-662 Warsaw, Poland*
(Received 13 December 2000; published 24 May 2001)

We investigate the role of static disorder on defect energetics on examples of interstitial oxygen atoms in amorphous (a)-SiO_2. We generate representative amorphous structures using molecular dynamics with empirical potentials and refine them using the periodic plane-wave density-functional method (DFT). We calculate the DFT distribution of incorporation energies for 96 peroxy-linkage (PL) configurations in a periodic model of a-SiO_2. The calculations show a big site-to-site variation of incorporation energies. We partition the oxygen atom incorporation energy into contributions from a small local cluster around the defect and from the rest of the amorphous network. The striking result is that the incorporation of a defect can create as well as release the strain energy in the embedding network. The variation of the PL incorporation energy is dominated by the contribution from the surrounding amorphous network, with the distortion of the local geometry of the defect contributing only about one third of the total variation. The two contributions are statistically independent. Our results provide an analysis of the distribution of defect incorporation energies in a-SiO_2 and emphasize the importance of disorder and statistical approaches, which cannot be achieved in crystalline and cluster models of amorphous structure. Additionally, since the defect energies can be so strongly dependent on the longer-range strain fields, amorphous samples prepared differently and hence having different distributions of strain may perform differently in applications.

DOI: 10.1103/PhysRevB.63.224207 PACS number(s): 71.55.Jv, 71.23.−k, 81.65.−b, 66.30.Lw

I. INTRODUCTION

Most studies (both experimental[1] and theoretical[2]) of disorder in the many amorphous silicon dioxides emphasize structure: topology, pair-correlation functions, and bond angle distributions. There is some work on trends in density and enthalpy,[3] or trends in diffusion constants and solubility for rare-gas atoms (see, for example, Refs. 4 and 5) and oxygen[6] in silica glasses. Far less has been done to understand the links between structure and the performance of optical fiber gratings and gate dielectrics, which depends on defect behavior. Our calculations show significant links between defect energetics and both local and (unanticipated in previous work) medium-range order.

Quantum-mechanical modeling done so far has concentrated on either α-quartz as a model or on the use of small defect clusters saturated by hydrogen atoms. The assumption that such clusters can represent the amorphous structure properly (see, for example Refs. 7 and 8) is questionable and has not been properly tested. Doubts about cluster calculations stem from continuing arguments about the roles of medium-range order and long-range forces associated with charge distribution in the system and also charged defect species. Our present work extends our recent periodic plane-wave density-functional (DFT) calculations, which focused on the properties of atomic and molecular oxygen species in different charge states (as potential oxidizing species) in α-quartz[9] and a-SiO_2.[10] Here, we examine the distribution of the defect energies and the role of short range and medium-range order in determining defect properties.

Structural disorder can affect defect properties, such as incorporation energies, electrical levels, and optical transitions. In this paper, we focus on the incorporation energy and structure of an extra oxygen atom in a-SiO_2 and the response of the embedding network upon incorporation of the defect. The oxygen atom is inserted into the Si–O–Si bond to form a peroxy linkage (PL),[7–9,11,12] and causes strong local and medium-range distortion of the network. Our recent periodic DFT calculations in a-SiO_2 (Ref. 10) show significant site-to-site dispersion in the oxygen atom incorporation energy. This dispersion characterizes both the amorphous structure (where the defect acts as a probe) and the defect properties in amorphous material (where static disorder introduces a variation in the defect environment as opposed to the crystalline structure). One of the main outstanding questions is the interplay between the geometry of the local structure around each particular incorporated oxygen atom (part of the network whose properties are changed by the presence of the defect) and the rest of the amorphous structure. Understanding this interplay should allow us to assess the applicability of crystalline and molecular cluster models for studies of such defect properties.

Our methods are described in Sec. II. First, we build realization of amorphous structures using classical molecular dynamics. We refine these structures using the same periodic plane-wave DFT methods as will be used for our calculations of the atomic oxygen species. The amorphous structures are then characterized in terms of angular, bond-length, and ring statistics. In Sec. III, we present the results of DFT calculations of all the possible peroxy linkages (PL's) formed on incorporating an oxygen atom in our amorphous supercell. *We find that the incorporation energy does not correlate with natural parameters of the local structure, such as the Si–O–Si angle.* In Sec. IV–VI we develop pair potentials to analyze the total energies from these DFT results into a local component due to the nearest-neighbor atoms and a contribution of the rest of the system. The pair potentials reproduce with high accuracy the DFT total energies of the dif-

ferent amorphous structures and the PL's. Our results show the major importance of relaxation of the surrounding amorphous network: the variation of the *local* contribution to the incorporation energy is only approximately *half* that of the surrounding network. One important result is that the oxygen incorporation and distortion of the local structure can *release* as well as *create* strain in the surrounding amorphous structure. This leads to either *positive* or *negative* contributions of the surrounding network to the relaxation energy on oxygen incorporation. This result casts doubt on the use of small molecular models for studying the incorporation of species in a amorphous structure. In a separate paper,[13] we shall compare the results from our periodic DFT calculations, molecular cluster calculations, and the use of the ONIOM technique,[14] in which the distortion of the amorphous structure surrounding the local molecular cluster is treated, at least in part.

II. GENERATION OF AMORPHOUS STRUCTURES AND THEIR PROPERTIES

To generate realizations of amorphous structures, we have used classical molecular-dynamics (MD) simulations, followed by static relaxation using periodic plane-wave DFT calculations. The DFT-relaxed structures were then used for defect calculations. We adopt a 72-atom unit cell, as in our previous DFT defect calculations. The results of MD simulations are known to depend on the cooling rate from the melt.[15] We therefore generated three different 72-atom realizations of amorphous silica using different quench rates. These structures are designated as amorphous 4, 5, and 6. Our classical molecular dynamics used a set of two- and three-body empirical potentials[16] which has been applied extensively to study crystalline, liquid, and amorphous phases of silicon dioxide, including densified[17–19] and porous silica.[20,21] Key properties calculated with this potential set (pair-distribution functions, static structure factors, vibrational densities of states,[22] bond angle distributions) agree well with neutron-diffraction and magnetic-resonance measurements. We adopt a slight modification of the procedure used in Ref. 16 to achieve smooth continuous quenching from 3000–1000 K.

The MD calculations were made for a cubic unit cell of side 10.29 to match the experimental density[23] of 2.20 g/cm.^{3} An initial α-quartz structure was slightly distorted to fit the cubic unit cell and then melted using MD. The liquid SiO_2 was simulated for 36 ps at 3000 K, followed by quenching from 3000–1000 K. The three quench rates used were 100 K per 8, 16, or 32 ps; particle velocities were scaled to decrease the temperature by 1 K every 0.08, 0.16, and 0.32 ps, respectively. The empirical potentials[16] reproduce the melting temperature of silica of about 1500 K well. For temperatures above 2000 K, self-diffusion is still significant, and the system has a chance to rearrange its geometry. Root-mean-square displacements of atoms were 3.93, 5.68, and 6.10 Å for the three simulation times, which suggests that the total MD run time in the liquid state sufficed to decorrelate the structure from the initial one. The system was then equilibrated at 600 and 300 K and quenched to 0 K by geometry relaxation. The total simulation times were 210, 360 and 680 ps. A check of the geometries showed the ideal connectivity in all cases.

The amorphous structures were then fully relaxed (including the lattice vectors and the volume of the unit cell) using the DFT VASP code[24] with generalized gradient approximation (GGA) and the PW91 functional,[25] and the plane-wave basis set with a 400-eV energy cutoff. We included only the *G* point in Brillouin-zone integration. Ultrasoft pseudopotentials were used for oxygen, and norm-conserving pseudopotentials for the silicon atoms. Geometry relaxation exploited conjugate gradient energy minimization. All relaxation procedures continued until forces on atoms were less than 0.05 eV/Å. The DFT relaxation energies for nondefective amorphous models were 1.5 eV on average per 72-atom unit cell (0.02 eV per atom), which corresponds to thermal kinetic energy at 180 K for this system. We found that by also relaxing atomic positions with fixed lattice vectors, approximately half of the relaxation energy is due to atomic-position changes and half due to volume relaxation. The extra relaxation upon changing from the empirical-potential method to DFT is merely a small ''shake'' without structural changes and corresponds to a kinetic energy of a small fraction of the melting temperature (below which the atoms exhibit only thermal movements without any topological changes). This suggests that the classical MD simulation has predicted a fairly deep local minimum.

We have also performed DFT MD calculations using the VASP code to test whether the final minimum-energy structures from the static DFT relaxation were the lowest. The calculations consisted of a DFT MD run, typically 0.5–1.0 ps at 600 K, and static relaxation of final geometries from these MD runs. In all cases the initial geometry was recovered (amorphous 4, 5, and 6), with the mean difference in atomic positions less then 0.05 Å and the energy difference smaller than 0.01 eV per unit cell. These very small differences are due to the flatness of the potential-energy surface near the minimum (a consequence of the soft Si–O–Si bending forces) and the finite precision of the relaxation.

Table I summarizes the properties of the amorphous model systems. The relaxed unit cells are almost cubic; the relatively small supercell size means some degree of deformation should be expected. The calculated densities are generally a little higher than those observed for vitreous silica (we note the tendency of DFT to overestimate the unit-cell volume), but the enthalpies and densities are well within the range identified for amorphous silicas by Navrotsky.[3] Amorphous silicas can have quite a wide range of densities, depending on the way they were formed. In our case, we are primarily concerned with the oxide of microelectronics.

The peak positions in the calculated radial distribution functions (1.634, 2.665, and 3.059 Å) agree well with experiment.[1,26]. Our structures have ring statistics with three- to eight-member rings in proportions similar to those in Refs. 15 and 27. However, three- and four-member rings are slightly overrepresented at the expense of eight-member rings, perhaps because of the slightly higher density. In summary, the generated systems appear to be fully acceptable representative models of amorphous silicon dioxide.

TABLE I. Calculated properties of a-SiO_2 models. $\langle R \rangle$ is the root-mean-square displacement of atoms during the total simulation time. The enthalpy gives the value per SiO_2 unit relative to α-quartz. In comparing the enthalpies and densities, it is necessary to correct for the tendency of the GGA functional to underestimate the density of SiO_2 materials.

Sample	Amorphous 4	Amorphous 5	Amorphous 6
Cooling rate	100 K/8 ps	100 K/16 ps	100 K/32 ps
Total time of simulation (ps)	210	360	680
$\langle R \rangle$ (Å)	3.39	5.68	6.10
E before DFT relaxation (eV)	−570.92	−571.03	−570.81
E after DFT relaxation (eV)	−572.12	−572.62	−572.32
$\lvert a \rvert$ (Å)	10.19	10.07	10.43
$\lvert b \rvert$ (Å)	10.19	10.61	9.92
$\lvert c \rvert$ (Å)	10.55	10.06	10.02
Volume (Å^3)	1091.72	1073.13	1036.33
Density (g/cm^3)	2.20	2.23	2.31
Enthalpy (eV)	0.16	0.14	0.15

III. ENERGETICS OF PEROXY-LINKAGE DEFECTS

Atomic oxygen in α-quartz and in a-SiO_2 forms a peroxy linkage (PL).[7–12] There are two stable PL forms (Fig. 1); they are related approximately by rotation of the Si–O–O–Si complex about the line joining the two Si ions. These configurations have different energies in general. In α-quartz, the energy difference between the two configurations is 0.18 eV, with a barrier of 0.57 eV for rotation of the –O–O– complex from the lower-energy configuration to the higher-energy one. The atomic oxygen-incorporation energy in the lowest-energy configuration is 2.03 eV (relative to the nondefective α-quartz structure and half of the energy of an isolated oxygen molecule). The formation of a peroxy linkage distorts the surrounding network, the distortion decaying with distance from the defect. In amorphous structures there are also two stable configurations of PL per site, but their incorporation energies have a characteristic distribution with a big spread around the average value.

We have concentrated on the lowest-energy amorphous structure, amorphous 5, to study oxygen atom incorporation.

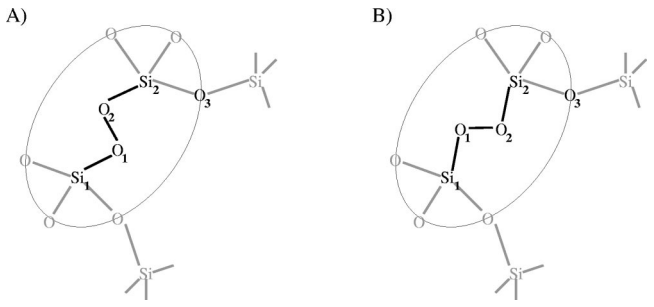

FIG. 1. Stable configurations of peroxy-linkage defect in SiO_2. There are two stable configurations with different incorporation energies for O inserted in a given Si–O–Si bond. The two geometries are approximately related by rotation of the –O–O– complex along the line connecting the two Si atoms. The oval represents schematically the partition into the local part and the rest of the system, since the detailed partition, described in the text, is given in terms of bonds and interatomic distances.

In this unit cell, the PL defects are separated by more than 1 nm. Calculations have been made for both configurations of the oxygen atom incorporated at each of the 48 different oxygen sites in our unit cell. The distribution of incorporation energies (Fig. 2) shows values centered on 1.9 eV, varying slightly asymmetrically from about 1.1–2.7 eV. Some of this variation is due to the inclusion of both low- and high-energy structures. Most PL defects have incorporation energies between 1.5 and 2.3 eV. However, in some cases it takes either much smaller or much larger energy to incorporate an oxygen atom. The incorporation energies in α-quartz of 2.03 and 2.21 eV are slightly above the mean for amorphous structure. The discrepancy between amorphous and α-quartz can be much bigger for other oxygen species in SiO_2.[10] One immediate conclusion is that α-quartz can be a poor oxide mimic and cannot, for example, be *a priori* assumed to give energies valid for describing silicon oxidation.

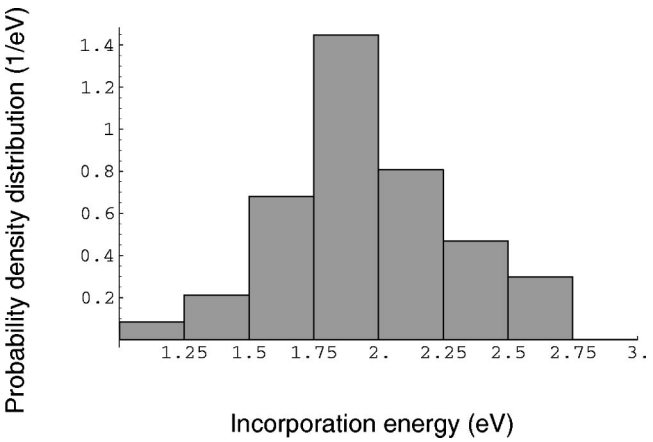

FIG. 2. Histogram of the probability density distribution of PL incorporation energies. Energies for both configurations (high and low energies) at each site are included. The incorporation energy is the difference between the energy of the stable defect structure and the sum of that of the initial amorphous structure and half of the isolated oxygen molecule. Corresponding values for α-quartz are 2.03 and 2.21 eV.

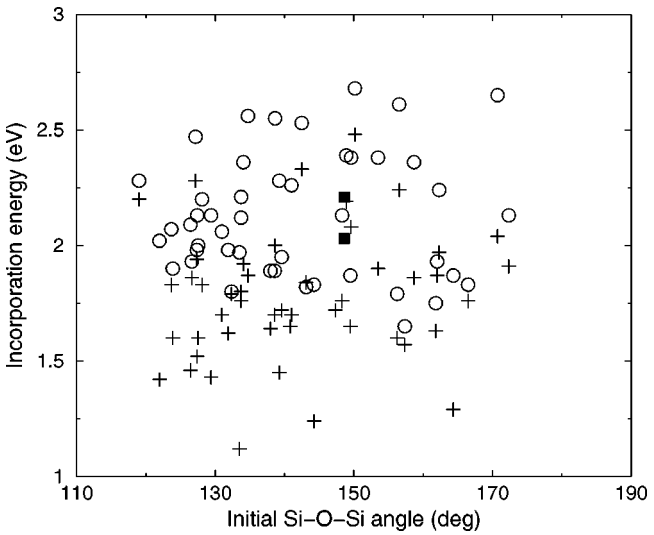

FIG. 3. Incorporation energy of the peroxylinkage as a function of the initial Si–O–Si angle. The low-energy configurations in the amorphous sample are plotted as ''+;'' the high-energy ones as '''o.'' The full squares represent the results for α-quartz. There is a negligible correlation between the initial angle and the PL incorporation energies.

The large dispersion in the incorporation energies suggests that in a-SiO_2, the atomic displacements due to defect formation may trigger additional rearrangements in the medium-range structure, which can produce or release strain in the network. This appears to be true even without the changes in topology (connectivity) that can occur, perhaps by diffusion, at higher temperatures. We have seen no signs of other possible low-energy structural reorganizations, such as those suggested for silicates[28,29] or found in simulations of plastic deformation in a-C:H.[30]

The energy dispersion does not originate solely from the local geometry of particular oxygen sites. For example, there is a complete lack of correlation between incorporation energy and the initial Si–O–Si angles of the corresponding oxygen sites (Fig. 3). We have tried other characteristics, such as the torsion angle of Si–O–O–Si, the size of the minimal ring containing the defect, the distribution of minimal rings, the distribution of all rings containing the defect, and finally the electrostatic potential at the oxygen atom of the initial site. In no case we did find a correlation with the PL incorporation energy. Interestingly, there is a clear correlation between the initial Si–O–Si angle and the torsion angle of peroxy linkages, shown in Fig. 4. It is striking that even though the geometry of the initial site determines the geometry of the defect with good accuracy, there is no simple dependence of the incorporation energy on these angles.

IV. STRUCTURE OF THE PEROXY LINKAGE AND ITS RELATION TO THE STRAIN ENERGY OF THE SURROUNDING NETWORK

We may compare interatomic distances for the peroxy linkage with corresponding spacings for the initial, nondefective site. Table II shows both average values and their root-mean square spread. The bonds Si_1–O_1 and O_1–O_2 for PL (see Fig. 1) are essentially rigid showing a very small dispersion of length. The Si_1–O_1 bond increases its length slightly on defect formation. On the other hand, the Si_1–O_1–O_2 and O_2–Si_2–O_3 angles appear to be rather flexible, as reflected in the distances Si_1–O_2 and O_2–O_3 having large dispersion compared with that for amorphous 5. The most noticeable difference between the non-defective and defective networks is in the Si_1–O_3 and Si_1–Si_2 distances. Incorporation of oxygen into a network increases the distances on average by 0.45 (Si_1–O_3) and 0.58 Å (Si_2–Si_2). The rms spreads of distances become larger for larger interatomic spacings, at least up to 4.3 Å (ultimately, for large distances, the change must tend to zero) suggesting that medium-range order could be important.

These large displacements, as well as new constraints on the angles due to the *changed bonding structure of the network*, must be accommodated by the surrounding network.

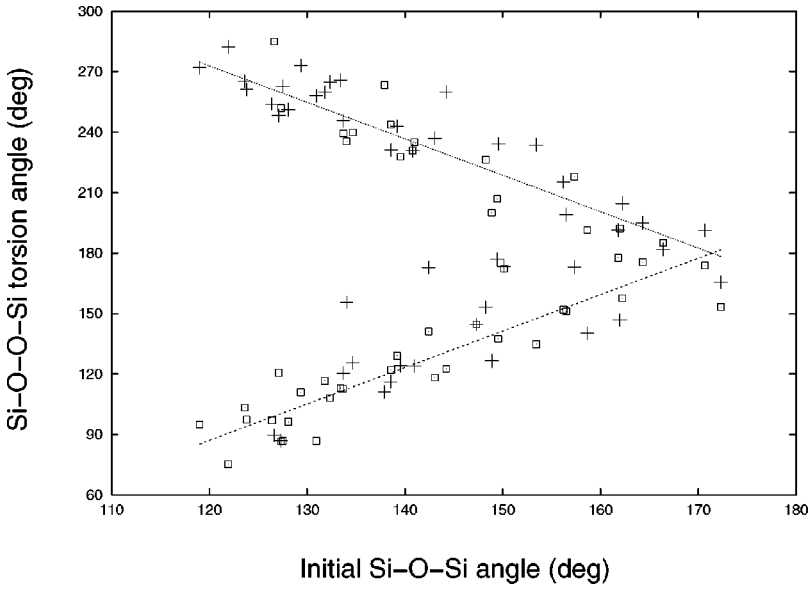

FIG. 4. The relation between the initial Si–O–Si angle of the nondefective system and the Si–O–O–Si torsion angle of the relaxed peroxylinkage defect incorporated into the amorphous sample. The low-energy configurations are plotted as squares, the high-energy ones as ''+.'' The lines are from the least-squares fit to all the points; they are $y=489.8°-1.807x$, and $y=-129.8°+1.807x$.

TABLE II. The distribution of selected interatomic distances (for atom labels, see Fig. 1) before and after incorporating a peroxy linkage. The results are based on calculations for all 48 different sites and for both high- and low-energy configurations at each.

	Peroxy linkage		Initial non-defective site	
Distance	Mean value (Å)	rms spread (Å)	Mean value (Å)	rms spread (Å)
Si_1-O_1	1.664	0.010	1.633	0.117
O_1-O_2	1.486	0.014		
O_2-O_3	2.642	0.136	2.663	0.082
Si_1-Si_2	3.637	0.197	3.059	0.117
Si_1-O_2	2.492	0.133		
Si_1-O_3	4.322	0.500	3.870	0.349
O_1-O_3	3.294	0.386		

We use the term *bonding structure of the network* to refer to the topology (connectivity) together with the characteristic properties of bonds (like the equilibrium distances, elastic constants, etc.), angular dependencies, and interrelations between them. In an empirical-potential description, the bonding structure of the lattice includes the topology and the potential set with its parameters. The actual bond lengths and angles can vary within certain limits, producing many realizations of the same bonding structure with different energies. Amorphous 5 is one example of a topology representative of a-SiO_2. We shall use the concept of bonding structure to divide the system into a local part and an embedding network. The local cluster comprises all atoms for which the bonding structure is changed, either in terms of topology or bonding properties. The rest of the system, the embedding network, preserves its original bonding structure on incorporation of the PL defect, but will undergo deformation. The change of certain interatomic distances and effective local elastic properties (the change in the rms spread of distances) due to the incorporation of the PL defect has an important effect on the embedding amorphous network, *allowing or forcing* it to access geometries that were not accessible for the nondefective network without breaking the bonds, rebonding, or accepting a large energy penalty for overstretching of the bonds and angles. This effect allows the defect to *lower* as well as *increase* the strain energy of the embedding network, even though the nondefective structure is at its energy minimum.

The key to understanding this phenomenon is recognizing that incorporating a defect, such as peroxy linkage, into an amorphous network relaxes some of the constraints and introduces new ones. Adding O replaces part of the network with a new, different network and neither the whole new network nor its parts are at the minimum of energy *given the new bonding structure*. Relaxation of the new system will lead to a new minimum of energy, one for which the embedding network can have strain energy either *higher* or *lower* than that of the initial nondefective network. The incorporation energy is likely to be higher if the defect increases interatomic distances in an already locally compressed region or lower if it relaxes an initially tensile strain by allowing some distances to increase. The effective ''softening'' of the local cluster (the bigger rms spread for Si_1-O_3 and Si_1-Si_2) will also allow for more relaxation in the embedding lattice.

V. PAIR POTENTIALS AS A TOOL FOR PARTITIONING THE ENERGY

We now wish to analyze the contributions to oxygen-incorporation energies from different parts of the amorphous network, and in particular, to partition the total energy into contributions from two regions, as outlined in Sec. IV. One region is the local cluster, that contains the defect; the other is the embedding network. To do this, we need short-range potentials mimicking the DFT energy surface for the defective systems. We can use a two-step approach. First, we derive a set of potentials for the defect-free system, used later to evaluate the response of the embedding network to the incorporation of a defect. Second, in Sec. VI, we derive a specific set of potentials describing the energy dependence of peroxy linkage on its local geometry. In this paper we deal only with neutral defects. For a charged defect the polarization of the host network can be long range. In this case the same analysis can be applied, but only when extended to include the response of the network to the external electric field.

First, we have considered several different ways to represent the potential energy of the nondefective network in terms of interatomic potentials, both pairwise and angle dependent. To fit the parameters of these potentials, we sampled the potential-energy space by generating about 600 configurations using DFT MD at 300 and 600 K, starting from the equilibrium geometry amorphous 5. Half of the configurations were taken from the beginning of the 300 and 600 K simulations to sample configurations close to the minimum. The other 300 configurations were chosen from the end of the 1-ps MD run at 300 K, when some equilibration of energy had taken place. Potential parameters were obtained by a least-squares fit to these energies. We have examined harmonic and third-order potentials between atoms, but found that including third-order terms made no significant improvement. Surprisingly, there was a significant improvement of the fit on replacing the angle-dependent contributions for Si–O–Si and O–Si–O [in the form $E = c(\cos\alpha - \cos\alpha_0)^2$] by harmonic Si–Si and O–O potentials, respectively. Table III gives the parameters of the minimal set of harmonic potentials that reproduces the DFT energy surface satisfactorily for the chosen set of 600 geometry con-

TABLE III. The minimal set of harmonic potentials of the general form $c(d-d_0)^2$ for representing the energy of the SiO_2 defect-free amorphous network; d is the corresponding interatomic distance, c and d_0 are parameters. The atom numbers are shown in Fig. 5.

	c (eV/Å^2)	d_0 (Å)
Intratetrahedra		
Si_1-O_1	12.045	1.522
O_1-O_3	1.761	2.967
Intertetrahedra		
Si_1-Si_2	0.825	3.096
Si_1-O_3	0.137	3.786

figurations. The relevant atoms are defined in Fig. 5. Figure 6 is a correlation plot, comparing energies from the DFT MD run with those calculated using pair potentials. The rms energy error is 0.09 eV, with a correlation coefficient of 0.997 between the DFT energies and fitted ones. One could certainly improve the correlation by including more interactions with further neighbors, but the accuracy provided by these simple potentials is sufficient for our purposes.

VI. THE CHOICE OF THE LOCAL CLUSTER AND ANALYSIS OF THE ENERGY CONTRIBUTIONS

We want to use the pair-potential approach to partition the incorporation energy of PL into contributions coming from the local cluster around the defect and the embedding network. The incorporation of peroxy linkage leads to local changes in properties of the network. The spatial extent of these changes provides good criteria for the partition. Our calculated average interatomic distances in the vicinity of PL (some are shown in Table II) show that only first-neighbor distances are significantly affected by the presence of the defect. This suggests a possible partition of the system with a small local cluster shown, albeit approximately, as the part of the structure inside the oval in Fig. 1. The precise partition into a local part and the rest of the system employed in further calculations is defined in terms of bonds and interatomic distances. We choose the smallest possible local cluster, which includes all the interactions between Si_1, O_1, O_2, and Si_2, as well as all interactions equivalent to O_2-O_3. Interactions between the atoms outside and those in the local cluster are calculated using the potential derived for the nondefective amorphous network. All such interactions are assigned to the embedding network energy.

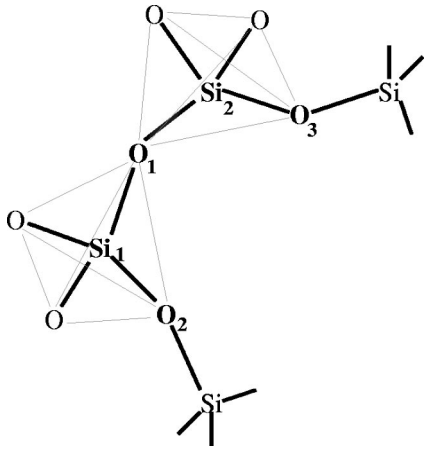

FIG. 5. Schematic diagram of the a-SiO_2 network. The numbering of atoms is used in defining the pairwise potentials (Table III).

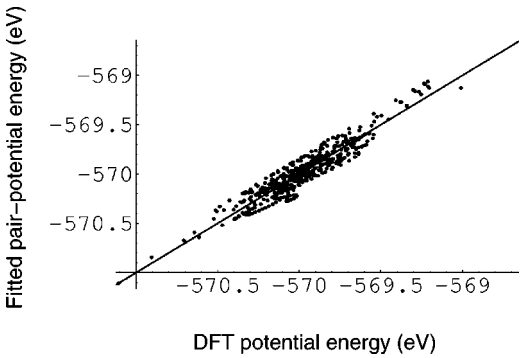

FIG. 6. Correlation plot for fitting a minimal set of harmonic potentials for the nondefective amorphous network. The correlation coefficient for the data is 0.997 and the root mean square error is 0.09 eV.

The division of the system has to capture the different properties of the two regions. Our choice of partition will meet this requirement if we can mimic the DFT incorporation energies of PL defects using this partition and the pair-potential approach. The total incorporation energy of peroxy linkage (E_{inc}) can be expressed as a sum of the local cluster energy (E_{loc}) and the change in strain energy (ΔE_{str}) in the embedding network ($E_{inc}=E_{loc}+\Delta E_{str}$). The embedding network comprises the whole system excluding the specific local cluster and it is different for each of the defect sites, of course. The change of strain energy is defined as the difference in potential energy of the embedding network after the incorporation and relaxation of PL and the potential energy evaluated for the same set of atoms in the initial nondefective amorphous sample. Since the embedding network is defect-free we can evaluate ΔE_{str} with the potential set for the nondefective amorphous network (Table III).

The local cluster, on the other hand, contains the defect and all bonds (and related atoms) in which properties are changed by the presence of the defect. Therefore, to describe this region we need a different set of potentials. The parameters for these potentials can be fitted to get the best agreement of the pair-potential incorporation energy with the DFT results. By doing several fits we established that the minimal set of harmonic pair potentials for the local cluster must include Si_1-O_1, O_1-O_2, and O_2-O_3 (atom numbering from Fig. 1). Since the incorporation of PL involves a change in the number of atoms in the local cluster, formation of a new bond and changes in other bonds, a constant energy term is needed to take care of the terms not represented by the harmonic pair-potential approach. The rms error of the fit is 0.09 eV, which is consistent with the error of the fit for the nondefective network. Again, adding more interactions with further neighbors improves the fit. Overall, it appears that the pair-potential approach has useful accuracy and can consis-

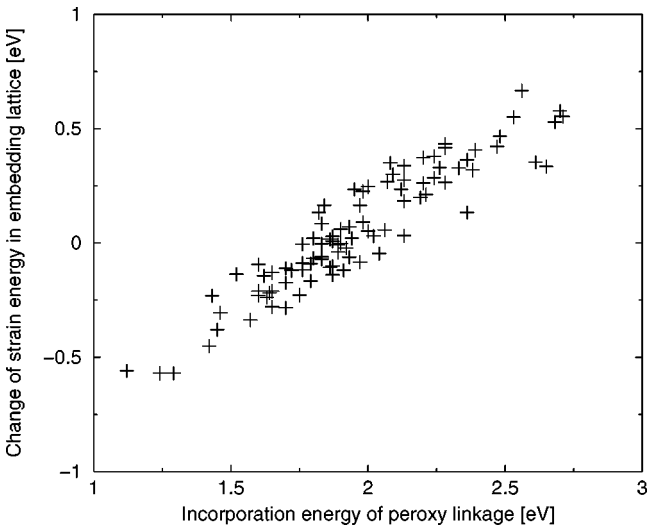

FIG. 7. Change in the medium-range strain energy as a function of peroxy-linkage incorporation energy. The clear correlation indicates that the change in strain energy is a dominant cause in the variation of the incorporation energy. Deviations from a linear relationship are due to variations in the local part of the energy. The correlation coefficient for the data on the graph is 0.94.

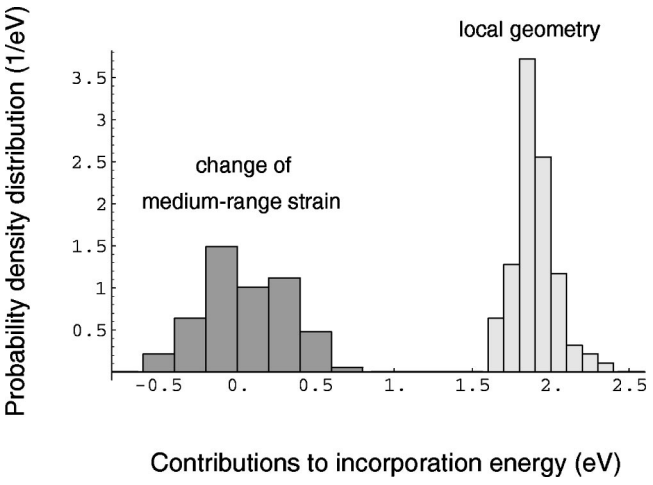

FIG. 8. Histograms showing the probability density distribution for the two contributions to the peroxy-linkage incorporation energy.

tently describe the variation of energy with the local geometry and the contribution of the embedding network. Therefore we conclude that our partition of the system into a local cluster and an embedding network successfully captures the different properties of the two regions. In particular the response of the embedding network to incorporation of the PL defect into the local cluster can be properly described by the pair-potential set for the nondefective a-SiO_2, derived in Sec. V.

Now we can analyze the contributions to oxygen-incorporation energy from the local cluster and embedding network. To avoid some of the fitting errors we shall use the DFT values for PL incorporation energy in all the following considerations. The oxygen-incorporation energies show a strong correlation of 0.94 with the change in the strain energy (ΔE_{str}) in the embedding network (Fig. 7) and give initial indications of the contributions of the two regions. The spread around a largely linear relationship is due to the variation of the local part of energy. The contribution from the local cluster can be simply evaluated as the difference between th incorporation energy of peroxy linkage and the change in strain energy in the embedding network (E_{loc} $=E_{inc}-\Delta E_{str}$). Table IV gives the characteristic parameters of the incorporation energy distribution and its contributions. The distributions of the strain and local part are shown in Fig. 8 and are quite different. The change in strain energy seems to be symmetrically distributed, whereas the distribution of local cluster energies is much more peaked around its mean value, with a tail towards high energies. The root-mean-square spread of changes in strain energy is approximately twice that of the energies of the local part. Further, the mean value of ΔE_{str} is close to zero, and the values can be positive or negative. Negative changes in strain energy were obtained for about half the oxygen sites in the amorphous structures considered in this work. The incorporation of additional oxygen atoms and the formation of a peroxy linkage can *create* as well as *release* strain in the amorphous structure in the vicinity of a defect.

We recognize that the partition into the local cluster and embedding network is not unique and will affect the relative spreads. We chose the cluster of the minimum size that can be used to model the PL defect. Therefore the size of the local cluster could only be increased. We can assess our choice by analyzing the combined probability density distribution of the local and embedding network (strain) contributions. Figure 9 shows the contour plot for the combined distributions. The two contributions appear almost independent. The small correlation coefficient of 0.33 is largely due to the few very high-energy PL configurations (simultaneous high

TABLE IV. Characteristic parameters of the distribution of peroxy-linkage incorporation energy (E_{inc}) and its partition into the local part (E_{loc}) and change in medium-range strain energy (ΔE_{str}). Note that $E_{inc}=E_{loc}+\Delta E_{str}$.

		Parameters of the distribution	
Energy	Method	Mean value (eV)	rms spread (eV)
Incorporation (E_{inc})	DFT	1.954	0.335
Change in medium-range strain (ΔE_{str})	Pair potentials	0.054	0.269
Local part (E_{loc})	$E_{loc}-\Delta E_{str}$	1.901	0.129

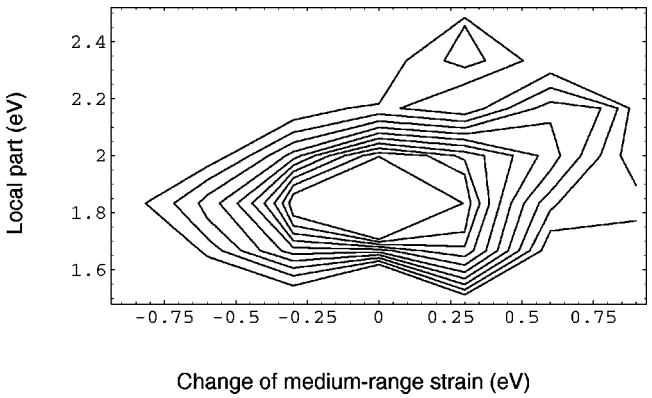

FIG. 9. The combined probability density distribution of the embedding network (change in strain energy) and local cluster energy components. A few very high-energy peroxy linkages (large positive values of both energies) are the source of the small correlation coefficient of 0.33. For these configurations there are alternative structures that usually have marginally lower energies.

local energy and high positive increase in strain energy). These can be regarded as the tail of the distribution. Moreover, these are the least likely PL configurations because of their very high-incorporation energy. Indeed, for these very high energy PL's we found there was also another type of stable configuration, similar in energy, but with a more compact structure. Such different structures can be marginally preferable energetically, since the compact structure leads to a smaller increase in strain energy, however at the expense of a higher contribution from the local part. We conclude that the local and strain (embedding network) contributions to energy are practically independent, with different distributions. They correspond to different regions of space, and the energies have largely distinct physical origins: one depends on the details of the local bonding of the defect, the other on the change in strain energy in the surrounding network. Most cluster calculations concentrate largely on just one of these energies, which limits their value.

VII. SUMMARY AND CONCLUSIONS

Our study of the site-to-site variations in the incorporation energies of peroxy linkages in a-SiO_2 leads us to four initial conclusions. First, one can generate realizations of a-SiO_2 by classical molecular dynamics followed by static DFT relaxation. These realizations, tested using DFT molecular dynamics, show good agreement with experimental data and with previous studies for distributions of bond lengths, angles, and ring statistics. In particular, the agreement with the experiment for enthalpy as a function of density gives us confidence that the amount of strain in the supercell is representative of real a-SiO_2. Second, we would like to emphasize that the site-to-site variations of defect properties in an amorphous material can be significant. Hence, proper characterization of a defect in amorphous material requires calculation of the distribution of values (mean value, spread, etc.) rather than just ''one number'' as in case of a defect in crystal. Third, analysis of the geometric and electronic structures of peroxy linkages at the 48 different oxygen sites of our 72-atom periodic cell points to a significant role of medium-range order. In particular, we show that it is possible to partition oxygen-incorporation energy into contributions from the local cluster around the defect and the change in strain in the embedding network (the response of the embedding network to the incorporation). Fourth, our results cast doubt on some of the standard approaches to modeling defects in a-SiO_2. For particular defect properties α-quartz can be a poor imitation of the amorphous oxide. Also, the terms from regions usually ignored in cluster calculations can be crucial in reproducing the defect properties accurately.

Perhaps more important, the results show a strong correlation between incorporation energies and changes in long-range strain energies. They show that distortion induced by incorporation of an oxygen atom and formation of a PL is statistically about as likely to introduce more strain into the region outside the nearest neighbors as it is to release the strain in the embedding amorphous structure. This is important, because it is the change in strain in the embedding network that dominates the large variations in incorporation energy. The amount of strain in the disordered structure will vary from sample to sample, and even within a volume of the sample. It will depend on the way the sample was formed, e.g., a very quick quench as opposed to a very slow quench. The implication is that amorphous samples prepared differently will have different distributions of incorporation energies (mean values, root-mean-square spread, and shape of distribution) and may perform differently in applications.

ACKNOWLEDGMENTS

M.A.S. would like to thank Fujitsu European Center for Information Technology for financial support. We are grateful to G. Pacchioni, J. L. Gavartin, and A. H. Edwards for useful discussions.

[1] A. C. Wright and R. N. Sinclair, in *Structure and Imperfections in Amorphous and Crystalline Silicon Dioxide*, edited by R. A. Devine, J.-P. Duraud, and E. Dooryhee (Wiley, New York, 2000), p. 121.

[2] L. W. Hobbs, C. E. Jesurum, and B. Berger, in *Structure and Imperfections in Amorphous and Crystalline Silicon Dioxide*, edited by R. A. Devine, J.-P. Duraud, and E. Dooryhee (Wiley, New York, 2000), p. 3.

[3] A. Navrotsky, Diffus. Defect Data **53/54**, 61 (1987).

[4] J.E. Shelby, J. Appl. Phys. **48**, 1497 (1977).

[5] J.E. Shelby, J. Non-Cryst. Solids **14**, 288 (1974).

[6] M.A. Lamkin, F.L. Riley, and R.J. Fordham, J. Eur. Ceram. Soc. **10**, 347 (1992).

[7] G. Pacchioni and G. Ierano, Phys. Rev. B **56**, 7304 (1997).

[8] G. Pacchioni and G. Ierano, Phys. Rev. B **57**, 818 (1998).

[9] A.M. Stoneham, M.A. Szymanski, and A.L. Shluger, in *Ultrathin*

Dielectrics, edited by D. A. Buchanan, A. H. Edwards, H. J. von Bardeleben, and T. Hattori, MRS Symposia Proceedings No. 592 (Materials Research Society, Pittsburgh, 2000), p. 3; M.A. Szymanski, A.M. Stoneham, and A.L. Shluger, Microelectron. Reliab. **40**, 567 (2000); M. A. Szymanski, A. M. Stoneham, and A. L. Shluger, Solid State Electronics (to be published).

[10] A. M. Stoneham, M. A. Szymanski, and A. L. Shluger, Phys. Rev. B (to be published).

[11] D.R. Hamann, Phys. Rev. Lett. **81**, 3447 (1998).

[12] J.R. Chelikowsky, D.J. Chadi, and N. Binggeli, Phys. Rev. B **62**, R2251 (2000).

[13] M. A. Szymanski, A. L. Shluger, A. M. Stoneham, D. Ricci, and G. Pacchioni (unpublished).

[14] M. Svensson, S. Humbel, R.D.J. Froese, and T. Matsubara, J. Phys. Chem. **100**, 19 357 (1996).

[15] K. Vollmayr, W. Kob, and K. Binder, Phys. Rev. B **54**, 15 808 (1996).

[16] P. Vashishta, R.K. Kalia, and J.P. Rino, Phys. Rev. B **41**, 12 197 (1990).

[17] S. Susman, K.J. Volin, D.L. Prince, J.P. Rino, R.K. Kalia, P. Vashishta, G. Gwanmesia, Y. Wang, and R.C. Liebermann, Phys. Rev. B **43**, 1194 (1991).

[18] W. Jin, R.K. Kalia, P. Vashishta, and J.P. Rino, Phys. Rev. Lett. **71**, 3146 (1993).

[19] W. Jin, R.K. Kalia, P. Vashishta, and J.P. Rino, Phys. Rev. B **50**, 118 (1994).

[20] A. Nakano, L. Bi, R.K. Kalia, and P. Vashishta, Phys. Rev. Lett. **71**, 85 (1993).

[21] A. Nakano, L. Bi, R.K. Kalia, and P. Vashishta, Phys. Rev. B **49**, 9441 (1994).

[22] W. Jin, P. Vashishta, and R.K. Kalia, Phys. Rev. B **48**, 9359 (1993).

[23] L. Levien, C.T. Prewitt, and D.J. Weidner, Am. Mineral. **65**, 920 (1980).

[24] G. Kresse and J. Furthmuller, Phys. Rev. B **54**, 11 169 (1996).

[25] J.P. Perdew, J.A. Chevary, S.H. Vosko, K.A. Jackson, M.R. Pederson, and C. Fiolhais, Phys. Rev. B **46**, 6671 (1992).

[26] J.H. Konnert and J. Karle, Acta Crystallogr., Sect. A: Cryst. Phys., Diffr., Theor. Gen. Crystallogr. **25**, 702 (1973).

[27] J.P. Rino, I. Ebbsjo, R.K. Kalia, A. Nakano, and P. Vashishta, Phys. Rev. B **47**, 3053 (1993).

[28] E.M. Stolper and T.J. Ahrens, Geophys. Res. Lett. **14**, 1231 (1987).

[29] R. Jeanloz, Nature (London) **332**, 207 (1988).

[30] A.M. Stoneham, P.D. Godwin, A.P. Sutton, and S.J. Bull, Appl. Phys. Lett. **72**, 3142 (1998).